HYDROLOGICAL PROCESSES
Hydrol. Process. (2010)
Published online in Wiley InterScience
(www.interscience.wiley.com) DOI: 10.1002/hyp.7719

A comparison of peak and plate electrodes in electrical resistivity tomography: application to the chalky groundwater of the Beauvais aquifer (northern part of the Paris basin, France)

Lahcen Zouhri* and Pascale Lutz
HydrISE, Department of Geosciences, LaSalle Beauvais Polytechnic Institute, 19 Rue Pierre Waguet, 60026 Beauvais, France

Abstract:

Electrical resistivity tomography was used in order to explore an experimental site of the LaSalle Beauvais Polytechnic Institute (France). The test was conducted along a profile line of 315 m length, using 64 electrodes deployed at an inter-electrode spacing of 5 m, and the data were recorded using gradient, Wenner and pole–dipole arrays. The performance of plate electrodes (non-conventional flat-based) is compared with the performance of peak electrodes (conventional spike). The hydrogeophysical investigation of the chalk aquifer system of Beauvais shows that the performance of plate electrodes is satisfactory, leading to inversions of small root-mean-square errors. Peak and the plate electrodes were tested before and after injection of a salt tracer in the piezometer of the experimental site. The study demonstrates the usefulness of plate electrodes (efficient, less time consuming) and the possibility of aquifer characterization by a salt tracer. Copyright © 2010 John Wiley & Sons, Ltd.

KEY WORDS electrical resistivity tomography; peak and plate electrodes; groundwater; tracer; chalk aquifer; Beauvais; France

Received 1 December 2009; Accepted 18 March 2010

INTRODUCTION

Electrical resistivity methods were developed in the early 1900s and have been very widely used since the 1970s, primarily due to the availability of computers to process and analyse the data. Over the last decade, electrical resistivity tomography (ERT) has been extensively used in geophysical investigations (Dahlin, 2001). The most common applications of ERT are geothermal field exploration (Wright *et al*., 1985), geological mapping (Caglar and Duvarci, 2001), solute transport and modelling (Slater *et al*., 2000; Kemna *et al*., 2002; Chambers *et al*., 2004), hydrogeological properties (Dahlin and Owen, 1998. Pham *et al*., 2002; Cassiani *et al*., 2006; Flathe, 2006; Descloitres *et al*., 2008; Uhlenbrook *et al*., 2008; Koch *et al*., 2009), environmental research (Rogers and Kean, 1980; Van *et al*., 1991; Garambois *et al*., 2002; Daily *et al*., 2004; Sénéchal *et al*., 2005; Rings and Hauck, 2009) and archaeology (Tsokas *et al*., 2008). These techniques are used extensively in the search for suitable groundwater sources and also to monitor the groundwater pollution (Depountis *et al*., 2001; Garambois *et al*., 2002; Westbrook *et al*., 2005; Acworth and Jorstad, 2006; Greenhouse John and Monier-Williams, 2007; Johnson *et al*., 2007).

Fractured-rock environments contain contaminants in saturated and unsaturated zones in many areas of the world. Investigating the transport of contaminants and the recharge pathways in fractured and heterogeneous environments is an essential step for characterizing groundwater flow and recharge processes. The comprehension of the spatial repartition of contaminants in geologically complex aquifer systems requires hydrologeological and geophysical monitoring, which includes periodic measurements of the physical, chemical and electrical parameters of the subsurface.

As resistivity is a fundamental electrical property of rock materials and closely related to their lithology, fracturation saturation and fluid salinity, the determination of the subsurface distribution of resistivity from measurements on the surface can yield useful information on the structure and composition of buried formations, as well as the hydrogeology. A common method for carrying out such measurements involves the injection of an electrical current into the ground. The electrical resistivity methods are one of the geophysical techniques that allow description of the different lithologic areas as a function of depth, depending on their electrical property contrasts, thus providing a good indication of water-bearing formations (Guérin and Benderitter, 1995; Meheni *et al*., 1996; BenKabbour *et al*., 2004). The most successful and beneficial surveys have been in mining, groundwater and engineering applications. These methods have some limitations such as the limited depth of penetration depending on the maximal electrodes spacing. Thanks to its powerful and economical tool for groundwater exploration as well as the delineation of subsurface layer succession, the

* Correspondence to: Lahcen Zouhri, Department of Geosciences, LaSalle Beauvais Polytechnic Institute, 19 Rue Pierre Waguet, 60026 Beauvais, France. E-mail: lahcen.zouhri@lasalle-beauvais.fr

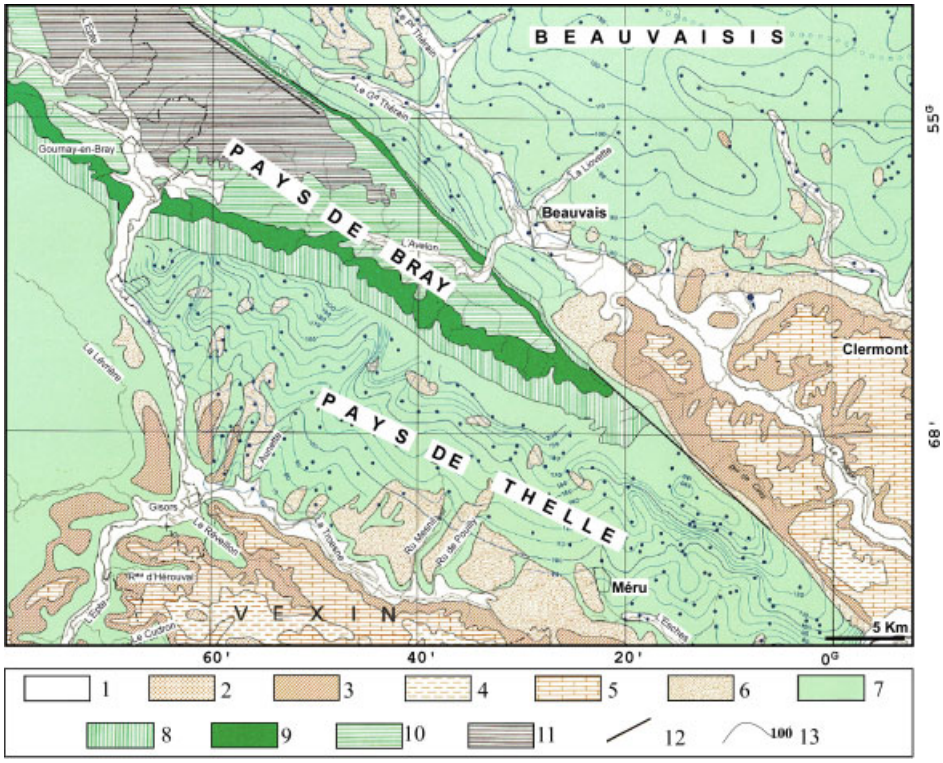

Figure 1. Hydrogeological map of the chalk groundwater of Beauvais (Paris basin): 1. Alluvions; 2. Oligocene and Miocene (sand, sandstone and marls); 3. Upper Eocene, 4. Lutetian (coarse limestone); 5. Cuisian-Sparnacian (medium sand and clay), 6. Thanetian (fine sand), 7. Senonian-Upper Turonian (Chalk with flint), 8. Cenomanian (glauconit chalk), 9. Albian (Clay of Gault (green sand)), 10. Neocomian (sand and clay), 11. Upper Jurassic (alternation of limestone and clay), 12. Fault, 14. Isopieze (After Roux and Tirat, 1967; modified)

vertical electrical sounding (VES) method has been used in many works, which can permit the determination of groundwater types (Kossinski and Kelly, 1981; Frohlich and Kelly, 1987; El-Waheidi *et al*., 1992; Matias, 2002; Toto *et al*., 2008) and subsurface structural features of water-bearing formations (Zouhri *et al*., 2004; Akaolisa, 2006).

It is convenient and customary for most resistivity techniques to define a response function called apparent resistivity, ρ_a, which can be estimated from surface measurements. The apparent resistivity represents the approximate mean resistivity value of the ground features investigated. The apparent resistivity values are thus related to the depth of penetration. Consequently, the apparent resistivity is a qualitative parameter and has to be inverted with the use of software to be interpreted.

The use of ERT techniques provides, after inversion of the apparent resistivity values, electrical resistivity two-/three-dimensional (2D/3D) images of the subsurface and has become an important tool for the electrical characterization of saturated/unsaturated zone and of aquifer basement. In this paper, we compare the performance of peak and plate electrodes in order to understand the variation of the resistivity in the saturated/unsaturated formations of the chalk aquifer of Beauvais (France). The ERT investigation described was also designed to image changes in resistivity before and after the injection of a salt tracer in the well of the experimental site of the LaSalle Beauvais Polytechnic Institute (IPLB) (France).

ELECTRICAL TECHNIQUES

Hydrogeological setting

In this article, we will report our investigations using the ERT technique. For the purpose of this experiment, a direct current source was used. The ERT survey was carried out using a multi-electrode system (ABEM Terrameter SAS 4000). The experiment was conducted in the hydrogeological experimental site of the Polytechnic Institute LaSalle at Beauvais. The aquifer of Beauvais (northern part of the Paris basin) is composed essentially of the Cenomanian units (Chalk), which rest on the Albian formations. The geological units are mapped in Figure 1. The aquifer basement is characterized by the Gault clay deposit (Albian). In practice, it is essentially the upper part, the Senonian chalk, that is captured. In the unconfined zone, the depth of the water varies between 50 and 60 m in the plains and less than 20–30 m in the humid valleys.

The Cenomanian chalk aquifer is characterized by a general groundwater flow towards the south and, more locally, towards the main drains of the Oise river valley.

The hydraulic gradient of the chalk aquifer is quite homogeneous and varies from 10 to 12‰. Its transmissivity ranges from 10^{-4} m^2/s at the centre of the plateau, 10^{-3} m^2/s in dry valley and 10^{-1} m^2/s in humid valleys (Nicolas and Wuilleumier, 2003). A general flow is observed to the south and more locally to the Oise river valley, the main drainage valley.

Well number	Lambert Coordinates X	Y	Depth (m)	Altitude (m)	Thickness (m)	Lithology
Campus Lasalle Beauvais 01024x0019/P Pz-1	580.86	1196.08	80	118	0 - 1,5 1,5 - 2 2 - 6 6 - 54 54 - 58 58 - 80	Silt Flint Clay Soft chalk Hard chalk Soft chalk
Campus Lasalle Beauvais 010244x0155/F2006 Pz-2	580.79	1195.86	102	115	0- 1,5 1,5- 2 2- 6 6- 54 54- 102	Silt Flin Clay Soft chalke White soft chalk
Campus Lasalle Beauvais 01024x0150/F/RC Pz-3	580.64	1196.12	60	118	2,5 - 60	White chalk with flint

Figure 2. Hydrogeological and lithological characteristics of wells dug in the experimental site of IPLB

The experimental site is characterized by three wells that have been dug for hydrogeological and agricultural research activities. Characteristics of the lithological units of the wells reveal a variation of chalky formations and spatial distribution of their thickness (Figure 2).

Rainfall is the most important source of groundwater recharge in the area, but laterally through the water infiltrated at the slopes (coteaux). A recharge by the Thérain river is possible but insignificant. The piezometric surface is characterized by seasonal variations: high water is usually reached in March–April, and low water between early October and the end of December. The annual water balance varies between 15×10^6 and 11.5×10^5 m^3/ year.

Experimental Methods

The ERT data were recorded using three different arrays: gradient, Wenner and pole–dipole (PDP) (Figure 3). Sixty-four electrodes were deployed along the profile line at an inter-electrode spacing of 5 m, so that the total length of the profile line measures 315 m (Figure 4). The two types of electrodes, i.e. peak electrodes and plate electrodes, were used in turn for the recording the data, and then these two results were compared. The peak electrodes were introduced into the soil at their two-thirds length; plate electrodes were placed on conductive mud on the soil. Plate electrodes consist of square flat steel plates (10 cm × 10 cm × 2 mm) similar to those described in Athanasiou *et al.* (2007). Processing and inversion of the apparent resistivity pseudo-sections were performed using the RES2DINV software (Loke and Barker, 1996; Loke, 1997). For each dataset, L_1-norm was used for the data misfit and the inversion was carried out using the L_1-norm (blocky) inversion method for the model roughness (Loke, 2004; Loke *et al.*, 2003). The method uses a finite difference modelling scheme for solving the 2D forward problem and blocky inversion method for inverting the processed ERT data. RES2DINV generates the inverted resistivity depth image for each type of electrode. The quality of inversion results was checked by monitoring the root-mean-square (RMS) error:

$$\mathrm{RMS} = \sqrt{\frac{1}{n^2}\sum_{i=1}^{n}\left(\frac{\log(\rho_{\mathrm{meas}_i}) - \log(\rho_{\mathrm{cal}_i})}{\log(\rho_{\mathrm{cal}_i})}\right)^2} \qquad (1)$$

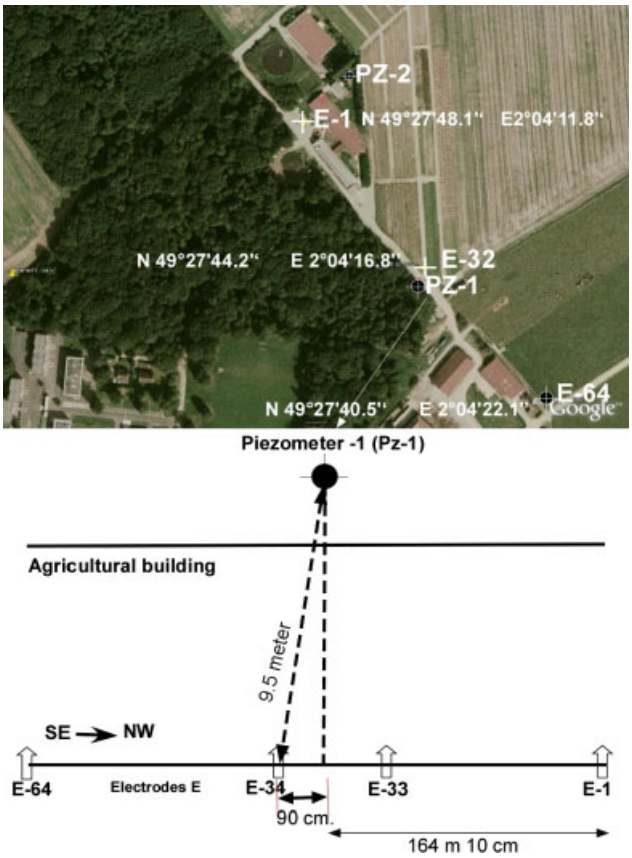

Figure 3. Location of the ERT profile and piezometer used in the experimental site of the LaSalle Beauvais Polytechnic Institute [PZ, piezometer; E-1 electrode 1 (Google Earth; modified)]

where ρ_{meas_i} is the measured apparent resistivity at the ith data point, ρ_{cal_i} is the calculated apparent resistivity from the resistivity section at the ith data point and n is the total number of measurement points.

One simple equation that gives the relation between the resistivity of a porous rock and the fluid saturation factor is Archie's law (1942). The electrical resistivity of a formation is proportional to the electrical resistivity of the saturating pore fluid and inversely proportional to the porosity raised to a power.

More precisely, the following relationship is presented in Reynolds (1997):

$$\rho = a\rho_{\mathrm{w}}\Phi^{-m}S^{-n} \qquad (2)$$

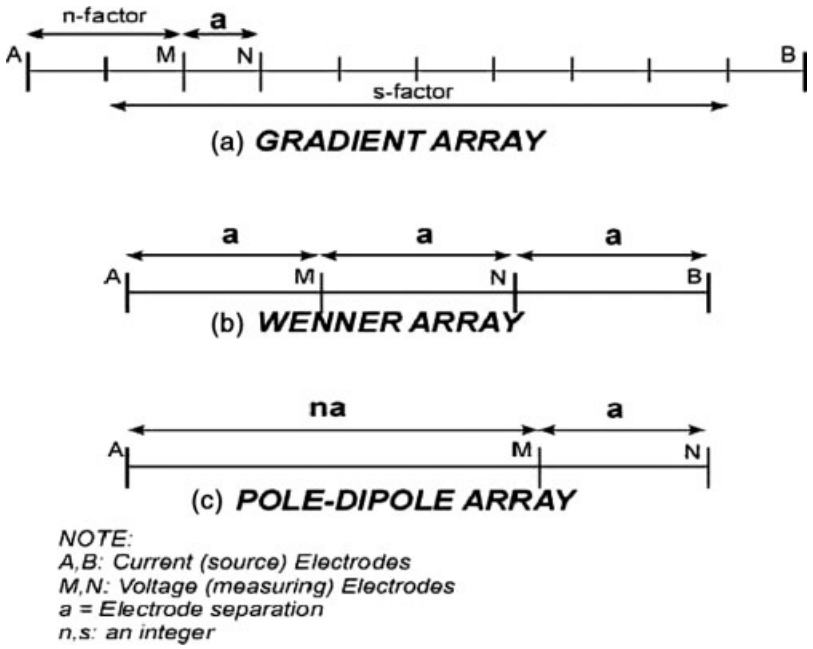

Figure 4. Sketch of the electrodes position for the (a) gradient array (s-factor = 8 and n-factor = 2); (b) Wenner array and (c) PDP array (n-factor = 2) (Reynolds, 1997)

where ρ and ρ_w are the effective rock resistivity and the resistivity of the pore water, respectively; Φ is the porosity; S is the volume fraction of pores with water and a, m and n are constants, where $0{\cdot}5 \leq a \leq 2{\cdot}5$; $1{\cdot}3 \leq m \leq 2{\cdot}5$ and $n \approx 2$.

The ratio ρ/ρ_w is the formation factor (F). One of the specialities of this study is the use of several arrays, each of which has some advantages and disadvantages (Figure 3; Reynolds, 1997). Generally, the larger the separation of the current electrodes, the deeper the penetration of the configuration; and the smaller the spacing of potential electrodes, the more the details of potential variation obtained. In practical applications, the selection of spacing a and separation s will be a trade-off between noise sensitivity, horizontal detail and depth penetration.

The Wenner array is relatively more sensitive to vertical changes and less sensitive to horizontal changes in the subsurface resistivity. However, the PDP array is an asymmetrical array and has relatively good horizontal coverage and is more sensitive to vertical structures. The PDP array requires a remote electrode, the 'B' electrode (Figure 4), which must be placed sufficiently far from the survey line (500 m in the present study). Because of its good horizontal coverage and great penetration depth, this is an attractive array for multi-electrode resistivity meter systems. However, the signal strength is lower compared to that of the Wenner array.

The gradient array allows achieving good resolution near the surface and has a relatively good horizontal coverage, but it has a penetration depth lower than that obtained with the PDP array.

The combination of the results obtained with these three arrays allows obtaining a good surface resolution and a great penetration depth.

The salt tracer was injected directly into the well in order to examine the performance of peak and plate electrodes, measure the spatial distribution of the electric resistivity in the chalk aquifer at several times after salt injection and estimate its dispersitivity features. The corresponding inversion paramaters for each array (gradient, Wenner, PDP) and the concatenate array obtained for several iterations before injection of the salt tracer are given in Table I.

ELECTRICAL SECTION

The ERT data for each array (gradient, Wenner, PDP) were inverted, without removing data points, using the peak (Figure 5) and the plate electrodes (Figure 6). The data obtained with the three arrays were concatenated and inverted, using the peak (Figure 7a) and the plate electrodes (Figure 7b). The corresponding inversion parameters are presented in Table I. The comparison of these results allows us to quantify the improvements due to plate electrodes in terms of the inverted resistivity sections and RMS errors. RMS error values after five inversions are weaker with the plate electrodes (3·8 and 3·1%, Figure 6) than with the peak electrodes (5·2 and 3·2%, Figure 5) for the gradient and Wenner arrays, respectively. The inverted ERT shows a heterogeneous vertical and horizontal distribution of the electrical resistivity values. The decrease of the resistivity with depth is in agreement with the groundwater level recorded at the piezometer (42 m). It is very important to mark the difference between the repartition of electrical resistivity resulting from the PDP array and peak and plate electrodes. Moreover, the RMS error values after inversion for the PDP array are higher with the peak electrodes,

Table I. Inversion parameters for the gradient, Wenner, PDP and concatenated arrays using the peak and the plate electrodes without removing bad datum points

Type of electrodes	Peak				Plate			
Array	Gradient	Wenner	PDP	Gradient + Wenner + PDP	Gradient	Wenner	PDP	Gradient + Wenner + PDP
Minimum electrode spacing	2·5	2·5	2·5	2·5	2·5	2·5	2·5	2·5
Number of data points	1252	437	588	2277	1252	437	588	2277
Number of layers in inversion model	14	18	22	17	14	18	22	17
Number of blocks in inversion model	1193	1538	2210	1662	1193	1538	2210	1662
RMS error after different iterations								
Iteration 1	9·93		11·62	12·04	10·43	10·94		10·89
Iteration 2	5·84		7·80	8·03	6·50	7·12		7·02
Iteration 3	5·00		6·88	7·03	5·68	6·31		6·18
Iteration 4	4·73		6·58	6·67	5·43	6·04		5·91
Iteration 5	4·60		6·41	6·49	5·29	5·89		5·76
Iteration 6	4·52		---	6·37	---	---		---
Iteration 7	4·46		---	---	---	---		---
Average block sensitivity	2·459	0·526	0·705	3·223	2·462	0·527	0·695	3·205

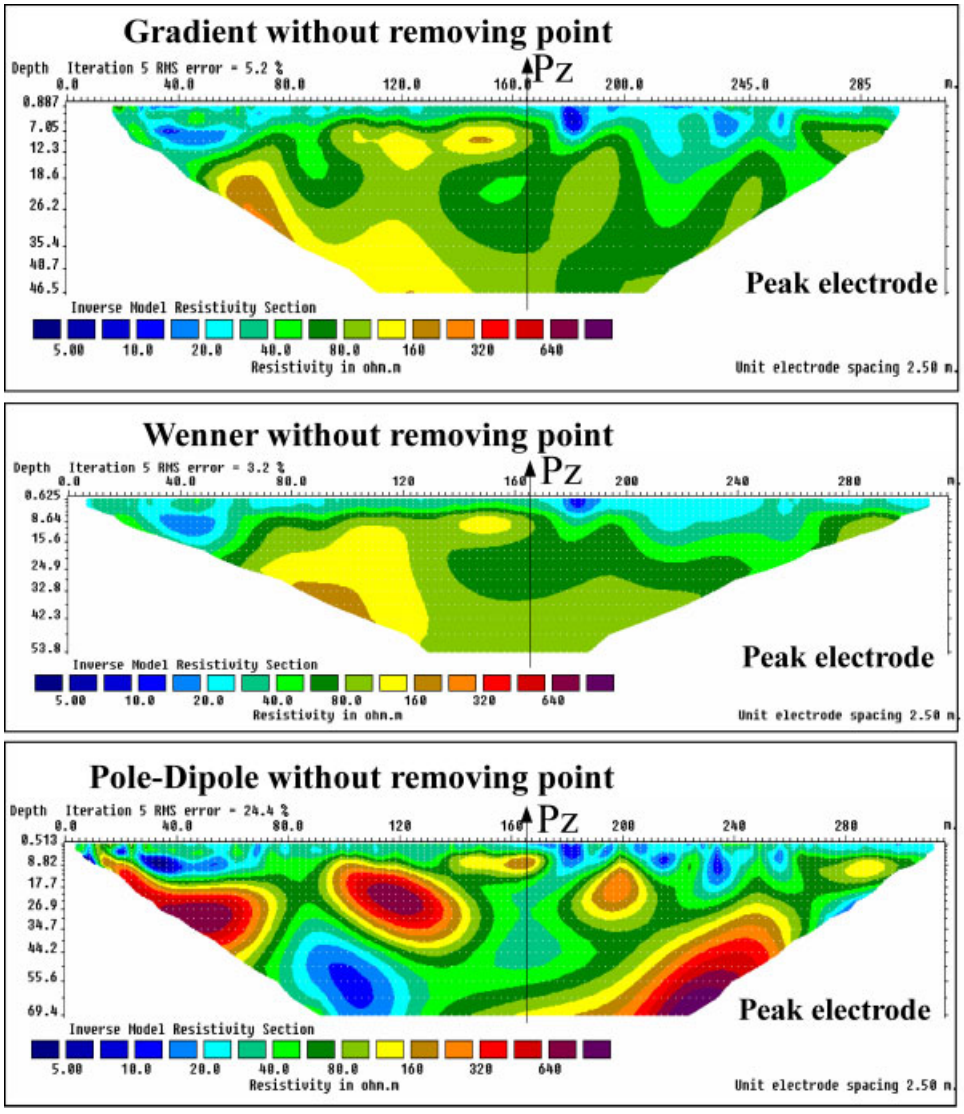

Figure 5. Inverted electrical resistivity tomography data using the peak electrodes without removing point before injection of salt tracer for the profile carried out at the experimental site of the IPLB. PZ, piezometer

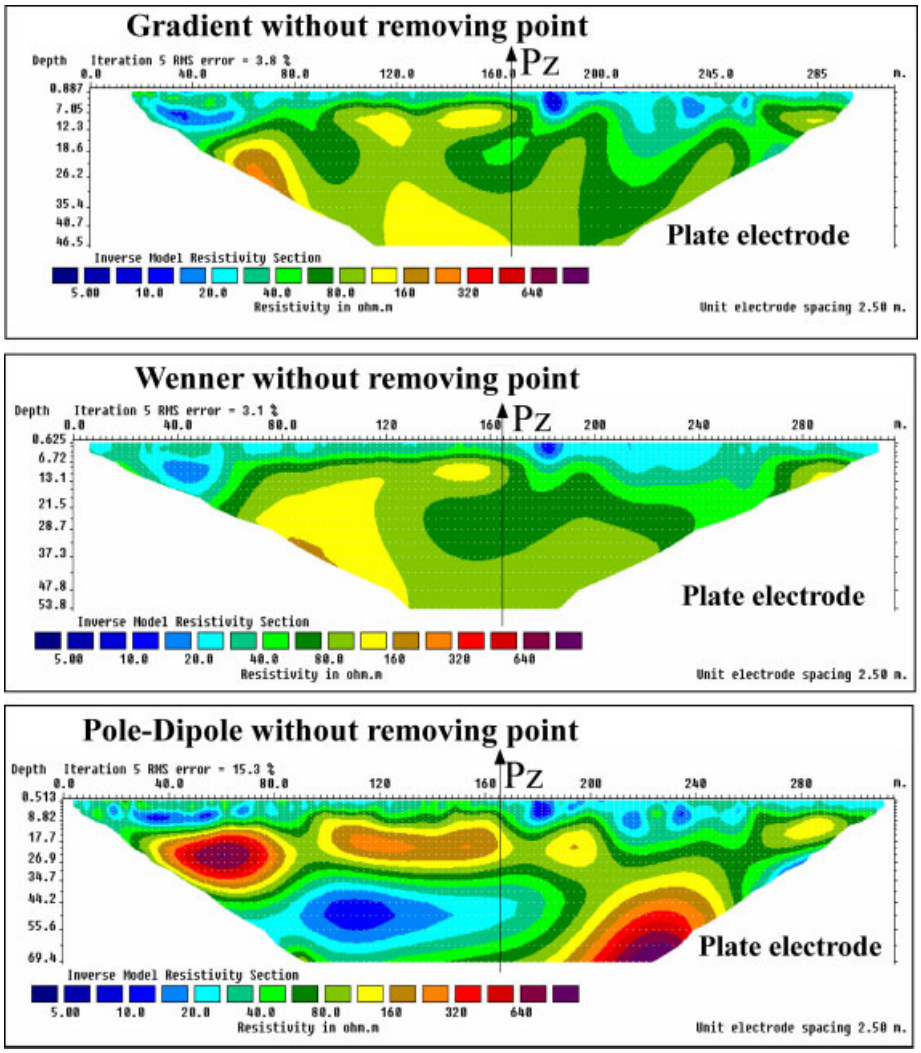

Figure 6. Inverted electrical resistivity sections using the plate electrodes without removing point before injection of salt tracer for the profile carried out at the experimental site of IPLB. PZ, piezometer

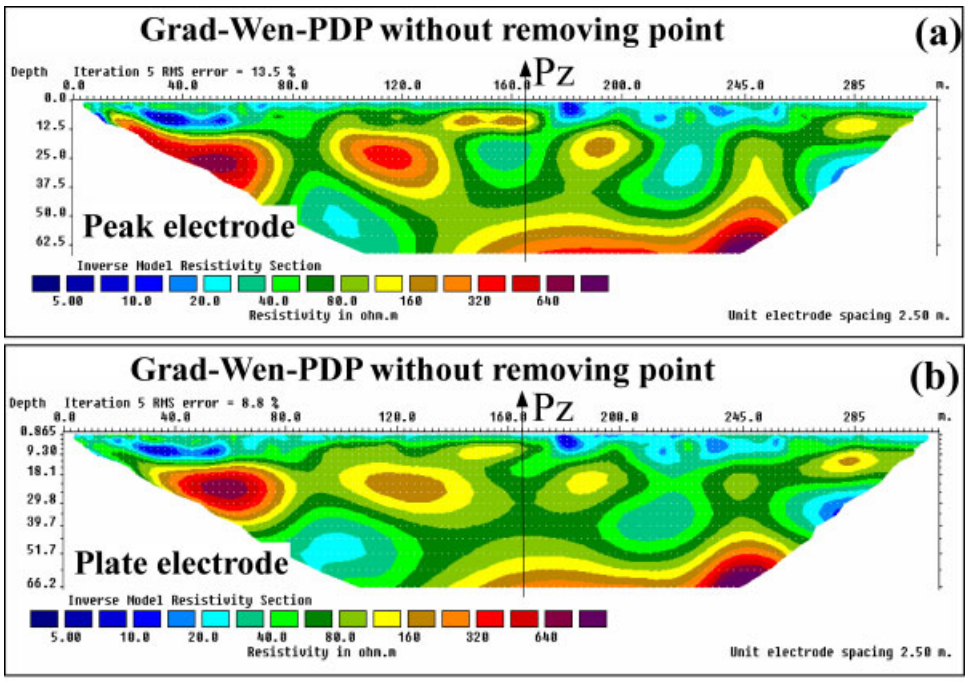

Figure 7. Inverted electrical resistivity sections for the concatenated array (gradient + Wenner + PDP arrays) using peak (a) and plate (b) electrodes, without removing point, before injection of salt tracer, for the profile carried out at the experimental site of the IPLB

Table II. Inversion parameters for the gradient (GRAD), Wenner (WEN), PDP and concatenated arrays, using peak and plate electrodes after removing some bad data points (cutoff = 30%)

Type of electrodes	Peak electrode				Plate electrode			
Array	GRAD	WEN	PDP	GRAD + WEN + PDP	GRAD	WEN	PDP	GRAD + WEN + PDP
Minimum electrode spacing	2·5	2·5	2·5	2·5	2·5	2·5	2·5	2·5
Number of data points	1216	437	516	2203	1252	437	536	2215
Number of layers in inversion model	14	18	22	17	14	18	22	17
Number of blocks in inversion model	1193	1538	2147	1613	1193	1538	2179	1624
RMS Error after different iterations								
Iteration 1	8·46	7·52	13·85	10·24	8·53	7·35	12·47	9·52
Iteration 2	4·29	4·07	10·24	5·89	4·76	3·88	8·91	5·16
Iteration 3	3·81	3·58	8·82	5·60	4·12	3·37	7·94	4·72
Iteration 4	3·80	3·38	7·93	5·20	3·89	3·18	7·60	4·71
Iteration 5	3·80	3·22	7·33	5·07	3·77	3·06	7·39	4·69
Iteration 6	—	—	—	—	3·69	2·98	—	—
Iteration 7	—	—	—	—	3·63	2·91	—	—
Average block sensitivity	2·384	0·526	0·620	3·223	2·462	0·527	0·632	3·205

about 24·4% (Figure 5) against 15·3% for the plate electrodes (Figure 6). Therefore, it can be observed that in this case the performance of the plate electrodes is much better than that of the peak electrodes. However, both the errors are quite high because of the fact that, in case of the PDP array, the second current peak electrode is located at infinity (the noise level is high). Using the plate electrodes and in the vicinity of the piezometer, the PDP model indicates a low-resistivity value (less than 40 Ω m). This low value corresponds to the groundwater of the chalk aquifer of the experimental site of Beauvais. Using the peak electrodes, resistivity values are in excess of about 30 and 80 Ω m.

The concatenation of the data acquired according to three arrays (gradient, Wenner, PDP) using both types of electrodes leads to two inverted models (Figure 7). By comparing Figure 7a and b, the RMS error after five iterations is less using the plate electrodes (8·8%) than using the peak electrodes (13·5%). Also along the profile line at some locations, the performance of the plate electrodes is better than that of the peak electrodes, leading to fewer bad data points.

To obtain resistivity models with lower RMS error values for the PDP array and thus improve the interpretation of the measurements, the bad data points were removed. More exactly, all data points corresponding to an RMS error of more than 30% were removed. This method was used because it allows us to compare the resulting sections under the same criterion and can be easily realized automatically by using RES2DINV software (Loke, 1997). Table II summarizes the principal features of the resulting sections.

Applying the 30% cutoff leads to the removal of 36 data points for the peak electrodes and none for the plate electrodes using the gradient array; 72 data points for the peak electrodes and 52 for the plate electrodes using the PDP array; 74 data points for the peak electrodes and 62 for the plate electrodes using the concatenate array. No points were removed using the Wenner array for both types of electrodes to achieve the 30% cutoff. In conclusion, it would be appropriate to mention here that the use of plate electrodes allows us to obtain datasets with less noise and leads to more precise inverted resistivity models. The performance of the plate electrodes is thus better than that of the peak electrodes.

While comparing Figures 8a and b, we can observe that the RMS error after five iterations is almost the same for both types of electrodes. But along the profile line at around 110–175 m, there is a zone of lower resistivity for the plate-electrode configuration. Therefore, using the PDP array, the plate electrodes are more effective in imaging low-resistivity anomalies corresponding to the aquifer.

INFLUENCE OF THE SALT TRACER ON THE UNDERGROUND WITH THE PEAK AND PLATE ELECTRODES

A salt tracer was chosen because it is not harmful to the environment. A salt tracer can create an electrical signature that allows qualitative monitoring with specific conductance probes and electrical resistivity surveys (Rugh and Burbey, 2008).

As mentioned earlier, there are two piezometers located in the study area. To monitor the contamination of groundwater, 1000 g of salt was introduced into the piezometer 1 (PZ-1, Figure 3) on 13 June 2009 at 13 : 40 h. This quantity was introduced inorder to visualize the contrast of the resistivity by using the peak and plate electrodes. After that, two sets of measurements were taken at two different times with both types of electrodes. The first step of the measurements was taken using plate electrodes, and second step with the peak electrodes. Experimental measurements were conducted using only the PDP array with an inter-electrode

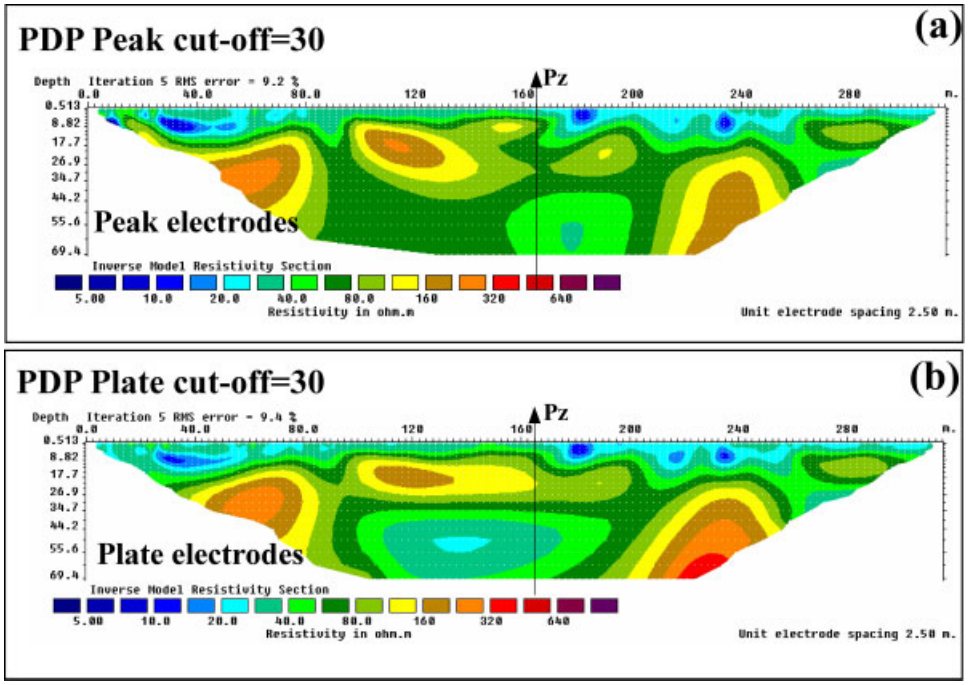

Figure 8. Inverted electrical resistivity sections for the concatenated array (gradient + Wenner + PDP arrays) using the peak (a) and the plate (b) electrodes, after removing point (cutoff = 30), before injection of salt tracer, for the profile carried out at the experimental site of the IPLB

distance of 5 m, because it allows the maximum depth of penetration among all the available arrays. Data points corresponding to an RMS error of more than 20% were removed in order to obtain low RMS errors and compare the sections under the same criterion. Figures 9 and 10 show the resistivity sections before and after the injection of salt, using the plate and the peak electrodes, respectively.

Before the introduction of salt, the comparison between sections using plate and peak electrodes reveals again the better performance of the plate electrodes to localize the chalk aquifer at a depth of 42 m, corresponding to resistivity values of less than 80 Ω m. The introduction of the salt tracer results in a decrease in the resistivity value of the chalk aquifer on all electrical sections. This decrease depends on the acquisition time and the electrode type. Using the plate electrodes, at 13 : 45 h, this decrease is about 20 Ω m from 110 to 180 m for a depth of more than 40 m, with a minimum value of 30 Ω m at the aquifer centre over 40 m. At 14 : 26 h, as this minimum value extends only up to 25 m, the salt pollution seems to slightly decrease. Using the peak electrodes, at 14 : 57 h, the low-resistivity anomaly corresponding to the salt pollution is about 40 Ω m over 60 m. At 15 : 37 h, this low-resistivity anomaly seems to be moving deeper and towards the NW. As a result, the effect of the salt is fading away as time passes (Table III).

In order to improve and complete this initial salt effect study, 2000 g of salt was introduced into the piezometer 1 (PZ-1; Figure 4) on 14 June 2009 at 11 : 20 h, and the electrical measurements were then conducted every half hour along the same profile line (Figure 4) using plate electrodes. The resulting inverted sections are presented Figure 11, after applying a cutoff of 20%. Comparing the sections launched at different times, it is obvious that the salt influence gradually increases to reach a maximum at 12 : 00 h. At this time, the low-resistivity anomaly is 20 Ω m againt 40 Ω m before salt introduction and is located from 120 to 170 m, at depths ranging from 40 to 60 m. At longer time, the salt pollution seems to be moving further, and the ground seems to be returning to a stable state from 13 : 40 h.

DISCUSSION AND CONCLUSION

The geoelectrical measurements performed at the experimental site of the LaSalle at Beauvais Polytechnic Institute (chalk aquifer) were conducted within the principal aim of quantifying improvements due to the use of plate electrodes in electrical tomography for hydrogeological applications. This study reveals that the measurements using plate electrodes are less noisy than those obtained with the usual peak electrodes for the gradient, PDP and concatenate arrays. Consequently, the use of plate electrodes allows us to remove fewer bad data points to reach the same RMS error and thus image the ground with more accuracy. Such results can be explained by the poor electrical contact between the peak electrodes and the soil due to the presence of flint. Moreover, using plate electrodes and the PDP array permits better detection of low-resistivity anomaly corresponding to the chalk aquifer.

After removing some data points from the dataset, the introduction of salt has shown a decrease of electrical resistivity values (Figures 9–11). Since the RMS errors after different iterations is too large, some points have

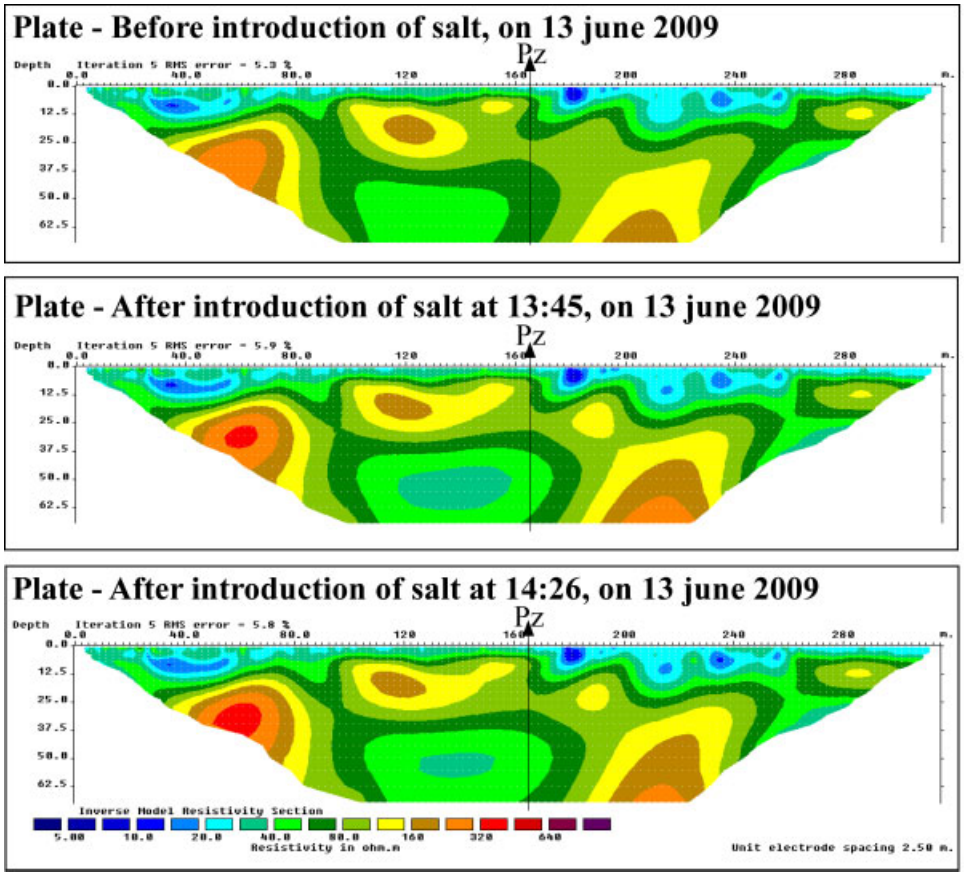

Figure 9. Spatial distribution of the electrical resistivity in the chalk aquifer using plate electrodes before and after injection of salt tracer into the piezometer PZ-1 (after removing some bad data points, cutoff = 20%). Salt injection at 13 : 40 h, on 13 June 2009

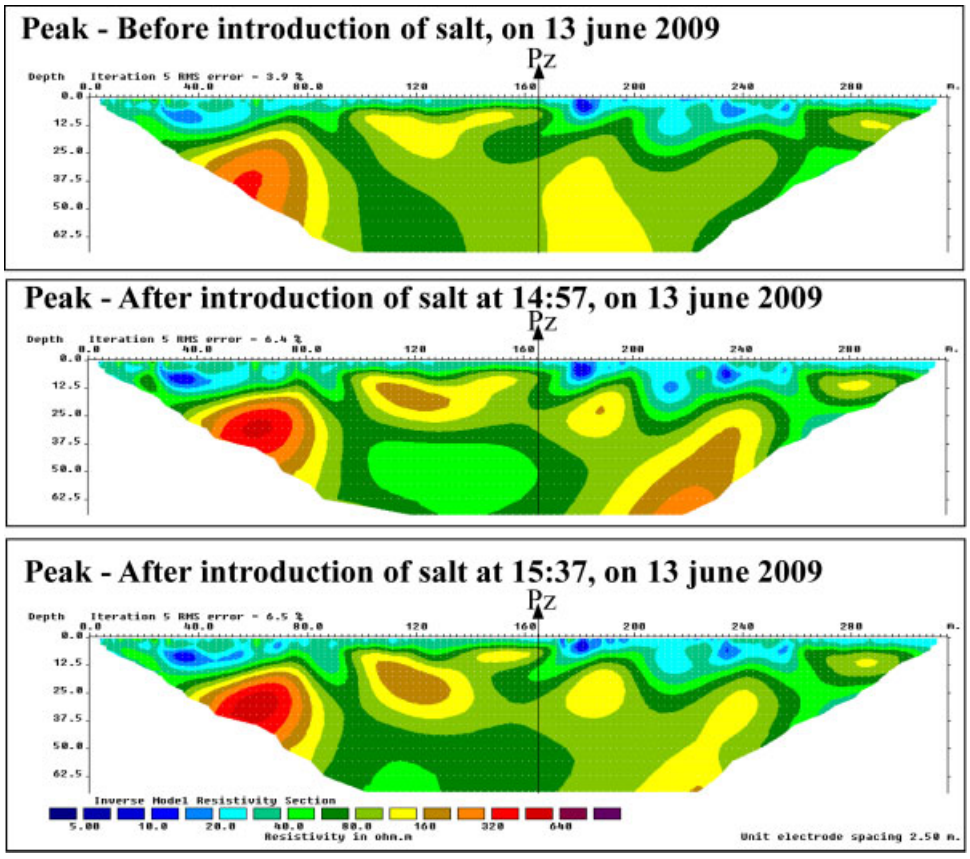

Figure 10. Spatial distribution of the electrical resistivity in the chalk aquifer using peak electrodes before and after injection of salt tracer into the piezometer PZ-1 (after removing some bad data points, cutoff = 20%). Salt injection at 13 : 40 h, on 13 June 2009

Table III. Characteristics of inversion ERT before and after injection of the salt tracer in piezometer PZ-1 for both electrodes (peak and plate) using the PDP array (Figure 3)

Type of electrodes	Peak			Plate		
Features	Before injection of salt	After injection of salt		Before injection of salt	After injection of salt	
Time (h)		14 : 57	15 : 37		13 : 45	14 : 26
Minimum electrode spacing	2·5	2·5	2·5	2·5	2·5	2·5
Number of data points	588	588	588	588	588	588
Number of layers in inversion model	22	22	22	22	22	22
Number of blocks in inversion model	2210	2210	2210	2210	2210	2210
RMS error after different iterations						
Iteration 1	9·93	18·23	23·27	11·48	12·90	13·73
Iteration 2	5·84	16·16	21·41	8·22	10·09	11·13
Iteration 3	5·00	15·55	20·79	7·55	9·42	10·47
Iteration 4	4·73	15·27	20·50	7·30	9·17	10·22
Iteration 5	4·60	15·08	20·31	7·17	9·02	10·07
Iteration 6	4·52	—	—	7·08	8·93	9·98
Iteration 7	4·46	—	—	7·02	8·86	—
Average block sensitivity	0·679	0·690	0·690	0·683	0·687	0·687

been removed from the dataset to remove any kind of discrepancies. In this case, the cutoff is 20. The removed points concern both peak and plate electrodes. After removal of the points, the RMS error decreased tremendously, which gave a better justification about the resistivity. After injection, the RMS error is about 6% (iteration number 6, Table IV) with peak electrodes against 5% with plate electrodes.

Note that the above survey was conducted in an environment complicated by anthropogenic features (pavement, metal pipes, etc.) with the expected high levels of measurement noise and modelling errors due to nature of the inhomogeneities. In Greece, the mean relative difference between the measured data pseudo-sections for standard and plate electrodes is about 2·3% (Athanasiou *et al*., 2007). This comparison was carried out in various environments (urban area: concrete, pavements, pavement stone, limestone (Athanasiou, *et al*., 2007) and monuments (Tsokas *et al*., 2008). In the archaeological domain, the inversions of the data showed higher RMS errors (5–15%) than what is normally expected (of the order of 2–3%) from conventional surveys. However, this error could be easily attributed to another source, namely the highly inhomogeneous near-surface stratum, a fact that violates the two-dimensional assumption inherent to the inversion scheme used (Tsokas *et al*., 2006, 2008).

The electrical signature is very complex in the chalk environment which constitutes heterogeneous aquifers. This poses some problem, in particular, in determining the groundwater flow in chalk aquifers systems. Dual-porosity fractured systems with around 1% and a matrix porosity of between 25 and 35% (Barker, 1993; Price *et al*., 1993) make it difficult to understand the electrical signature in unsaturated/saturated zones. The location of the water storage is in the irregularities on the fissure surfaces (Price *et al*., 2000), which can explain the spatial distribution of the electrical resistivity, notably in the unsatured zone.

The ERT survey performed in the chalk aquifer system indicates that the results obtained with plate electrodes are a reliable alternative to those from peak electrodes.

The RMS errors for plate electrodes are found to be less than that of peak electrodes without removing any point from the dataset. The inversions of the data showed higher RMS errors (3–18%), which could be easily attributed to the highly inhomogeneous formations (alteration) and the structure of the chalk aquifer resulting from the fractures.

Some problems were encountered when peak electrodes are used in the association with flint. Use of plate electrodes can extend the applications of geoelectrical techniques to environments that would not normally be suitable for resistivity tomography, but for this the arrangement for proper conduction of electricity will be needed such as by the use of a gel or mud. This suggests that arrays with a good signal-to-noise ratio (Wenner, gradient and PDP) are preferable for this type of survey. Moreover, tests with the three different electrode arrays indicate that the subsurface geoelectrical structures measured using peak and plate electrodes are clearly depicted.

Salt contamination of the groundwater in the piezometer of the experimental site of IPLB shows the utility and performance of plate electrodes for chalky aquifer system studies. However, it will be necessary to quantify these in a laboratory setting using ion chromatography and to determine the dispersion coefficient in the chalk aquifer of Beauvais.

ACKNOWLEDGEMENTS

The authors wish to thank the anonymous reviewers of this article for their useful comments and suggestions. The authors express their appreciation to Mr Christian Brault (responsible of LaSalle Beauvais farm), the technical service of LaSalle Beauvais Polytechnic Institute,

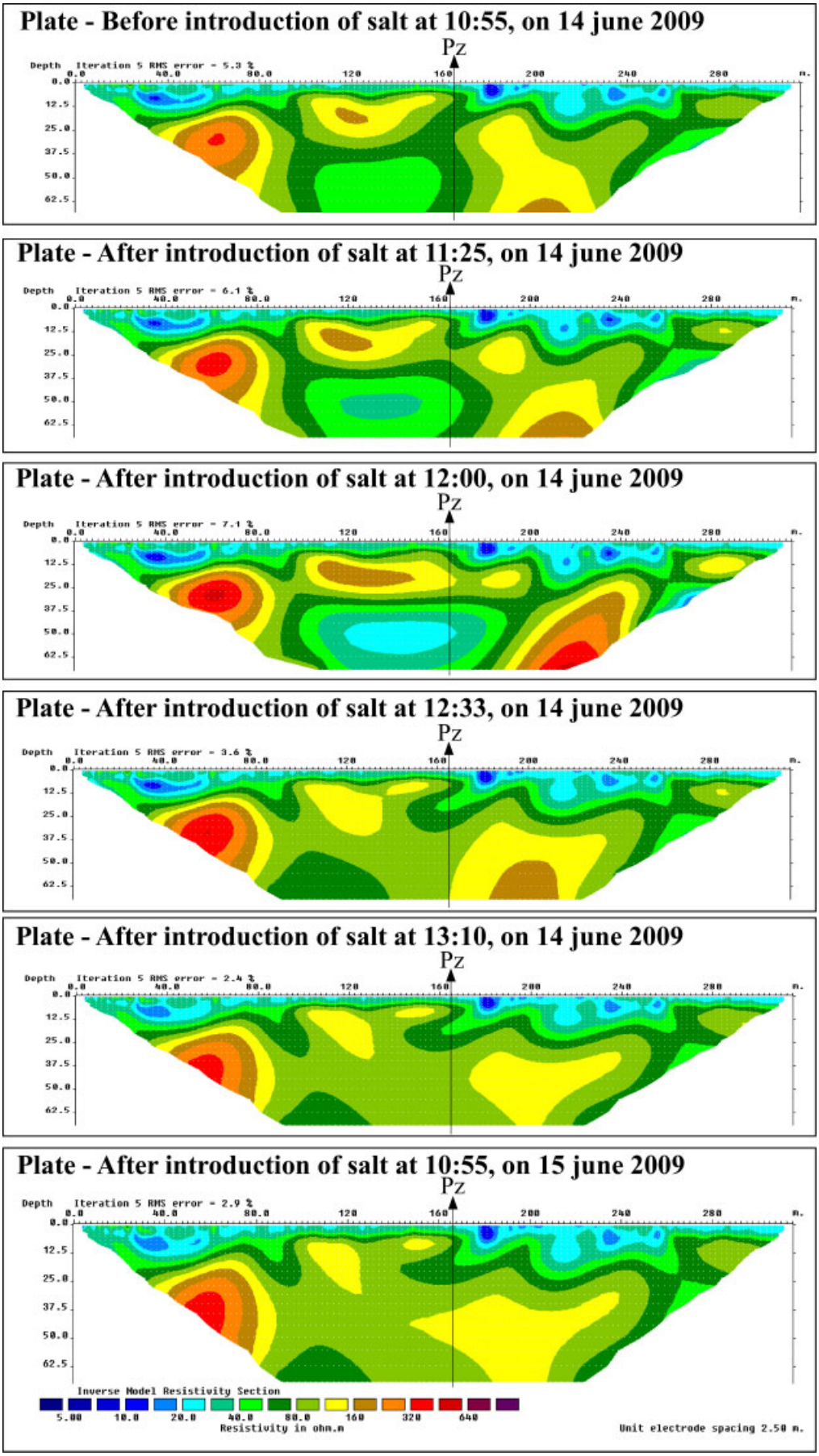

Figure 11. Spatial distribution of the electrical resistivity in the chalk aquifer using plate electrodes before and after injection of salt tracer into the piezometer PZ-1 (after removing some bad datum points, cut-off = 20%). Salt injection at 11 : 20 h, on 14 June 2009

Table IV. RMS errors of the inversion ERT with removing points data (before and after injection of salt)

Type of electrodes	Peak			Plate		
Features	Before injection of salt; cutoff = 0	After injection of salt		Before injection of salt	After injection of salt	
Time (h)		14 : 57	15 : 37		13 : 45	14 : 26
RMS errors						
Iteration 1	—	—	—	—	—	—
Iteration 2	9·93	11·62	12·04	10·43	10·94	10·89
Iteration 3	5·84	7·80	8·03	6·50	7·12	7·02
Iteration 4	5·00	6·88	7·03	5·68	6·31	6·18
Iteration 5	4·73	6·58	6·67	5·43	6·04	5·91
Iteration6	4·60	6·41	6·49	5·29	5·89	5·76
Iteration 7	4·52	—	6·37	—	—	—
	4·46	—	—	—	—	—
Average block sensitivity	0·679	0·65	0·61	—	—	—

and Kumar Aditya (for the award of a scholarship from the Indian Institute of Technology Kharagpur).

REFERENCES

Acworth RI, Jorstad LB. 2006. Integration of multi-channel piezometry and electrical tomography to better define chemical heterogeneity in a landfill leachate plume within a sand aquifer. *Journal of Contaminant Hydrology* **83**(3–4): 200–220.

Akaolisa C. 2006. Aquifer transmissivity and basement structure determination using resistivity sounding at Jos Plateau State Nigeria. *Environmental Monitoring and Assessment* **114**(1–3): 27–34.

Athanasiou EN, Tsourlos PI, Vargemezis GN, Papazachos CB, Tsokas GN. 2007. Non-destructive DC resistivity surveying using flat-base electrodes. *Near Surface Geophysics* **5**(4): 273–282.

Archie GE. 1942. Electrical resistivity as an aid in core analysis interpretation. *Transactions of the American Institute of Mining Engineers* **146**: 54–62.

Barker JA. 1993. Modelling groundwater flow and transport in the Chalk. In *The Hydrogeology of the Chalk of North-West Europe*, Downing RA, Price M, Jones GP (eds). Clarendon Press: Oxford; 59–66.

Benkabbour B, Toto EA, Fakir Y. 2004. Using DC resistivity method to characterize the geometry and the salinity of the Plioquaternary consolidated coastal aquifer of the Mamora plain, Morocco. *Environmental Geology* **45**(4): 518–526.

Caglar I, Duvarci E. 2001. Geoelectric structure of inland area of Gokova rift, southwest Anatolia and its tectonic implications. *Journal of Geodynamics* **31**: 33–48.

Cassiani G, Bruno V, Villa A, Fusi N, Binley AM. 2006. A saline trace test monitored via time-lapse surface electrical resistivity tomography. *Journal of Applied Geophysics* **59**(3): 244–259.

Chambers JE, Loke MH, Ogilvy RD, Meldrum PI. 2004. Noninvasive monitoring of DNAPL migration through a saturated porous medium using electrical impedance tomography. *Journal of Contaminant Hydrology* **68**(1–2): 1–22.

Dahlin T. 2001. The development of DC resistivity imaging techniques. *Computers and Geosciences* **27**(9): 1019–1029.

Dahlin T, Owen R. 1998. Geophysical investigations of alluvial aquifers in Zimbabwe. *Proceedings of the IV Meeting of the Environmental and Engineering Geophysical Society (European Section)*, Barcelona, Spain; 151–154.

Daily W, Ramirez A, Binley A, LaBrecque D. 2004. Electrical resistance tomography. *The Leading Edge* **23**: 438–442.

Depountis D, Harris C, Davies MCR. 2001. An assessment of miniaturised electrical imaging equipment to monitor pollution plume evolution in scaled centrifuge modelling. *Engineering Geology* **60**(1–4): 83–94.

Descloitres M, Ruiz L, Sekhar M, Legchenko A, Braun JJ, Mohan Kumar MS, Subramanian S. 2008. Characterization of seasonal local recharge using electrical resistivity tomography and magnetic resonance sounding. *Hydrological Processes* **22**(3): 384–394.

El–Waheidi MM, Merlanti F, Pavan M. 1992. Geoelectrical resistivity survey of the central part of Azraq basin (Jordan) for identifying saltwater/freshwater interface. *Journal of Applied Geophysics* **29**: 125–133.

Flathe H. 2006. Possibilities and limitations in applying geoelectrical methods to hydrogeological problems in the coastal areas of Northwest Germany. *Geophysical Prospecting* **3**: 95–110.

Frohlich RK, Kelly WE. 1987. Estimates of specific yield with the geoelectric resistivity method in glacial aquifers. *Journal of Hydrology* **97**: 33–44.

Garambois S, Sénéchal P, Perroud H. 2002. On the use of combined geophysical methods to assess water content and water conductivity of near-surface. *Journal of Hydrology* **259**: 32–48.

Greenhouse John P, Monier-Williams M. 2007. Geophysical monitoring of ground water contamination around waste disposal sites. *Hydrological Processes* **5**(4): 63–69.

Guérin R, Benderitter Y. 1995. Shallow karst network exploration using MT-VLF and DC resistivity methods. *Geophysical Prospecting* **43**(5): 635–653.

Johnson CD, Lane JW, Williams JH, Haeni FP. 2007. Application of geophysical methods to delineate contamination in fractured rock at the University of Connecticut landfill, Storrs, Connecticut, USGS; 15 pp.

Kemna A, Kulessa B, Vereecken H. 2002. Imaging and characterisation of subsurface solute transport using electrical resistivity tomography (ERT) and equivalent transport models. *Journal of Hydrology* **267**(3–4): 125–146.

Koch K, Wenninger J, Uhlenbrook S, Bonell M. 2009. Joint interpretation of hydrological and geophysical data: electrical resistivity tomography results from a process hydrological research site in the Black Forest Mountains, Germany. *Hydrological Processes* **23**(10): 1501–1513.

Kossinski WK, Kelly WE. 1981. Geoelectric sounding for predicting Aquifer Properties. *Ground Water* **19**: 163–171.

Loke MH. 1997. RES2DINV ver. 3.55 for Windows 98/Me/2000/NT/XP.

Loke MH. 2004. Tutorial: 2-D and 3-D electrical imaging surveys. Copyright (1996–2004); 139 pp.

Loke MH, Acworth I, Dahlin T. 2003. A comparison of smooth and blocky inversion methods in 2D electrical imaging surveys. *Exploration Geophysics* **34**: 182–187.

Loke MH, Barker RD. 1996. Rapid least-squares inversion of apparent resistivity pseudo sections by a quassi-Newton method. *Geophysical Prospecting* **44**: 131–152.

Matias MJS. 2002. Square array anisotropy measurements and resistivity sounding interpretation. *Journal of Applied Geophysics* **49**: 185–194.

Meheni Y, Guérin R, Benderitter Y, Tabbagh A. 1996. Subsurface DC resistivity mapping: approximate 1-D interpretation. *Journal of Applied Geophysics* **34**(4): 255–270.

Nicolas J, Wuilleumier A. 2003. Bassin de l'Aronde (Oise)—Suivi d'un réseau piézométrique d'usage dans la nappe de la craie. BRGM\51917-FR. BRGM consultable sur www.brgm.fr.

Pham VN, Boyer D, Le Mouël JL, Nguyen TKT. 2002. Hydrogeological investigation in the Mekong Delta around Ho-Chi-Minh City (South Vietnam) by electric tomography. *Comptes Rendus Geosciences* **3345**(10): 733–740.

Price M, Downing MA, Edmunds WM 1993. The chalk as an aquifer. In *The Hydrogeology of the Chalk of the North-West Europe*, Downing RA, Price M Jones GP (eds). Clarendon Press: Oxford, UK; 35–58.

Price M, Low RG, McCann C. 2000. Mechanisms of water storage and flow in the unsaturated zone of the Chalk aquifer. *Journal of Hydrology* **233**: 54–71.

Reynolds JM. 1997. *An Introduction to Applied and Environmental Geophysics*. John Wiley and Sons Ltd: Chichester; 796 pp.

Rings J, Hauck C. 2009. Reliability of resistivity quantification for shallow subsurface water processes. *Journal of Applied Geophysics* **68**(3): 404–416.

Rogers RB, Kean WF. 1980. Monitoring ground water contamination at a fly ash disposal site using surface resistivity methods. *Ground Water* **18**(5): 472–478.

Roux JC, Tirat M. 1967. Carte de la surface piézométrique de la nappe de la craie en Picardie. *Bureau de Recherches Géologiques et Minières, Service Géologique Régional Picardie Normandie*. Echelle 1/200 000.

Rugh D, Burbey T. 2008. Using saline tracers to evaluate preferential recharge in fractured rocks, Floyd County, Virginia, USA. *Hydrogeology Journal* **16**(2): 251–262.

Sénéchal P, Perroud H, Kedziorek M, Bourg A, Gloaguen E. 2005. Nondestructive geophysical monitoring of water content and fluid conductivity anomalies in the near surface at the border of an agricultural field. *Subsurface Sensing Technologies and Applications* **6**(2) 167–192.

Slater L, Binley A, Daily W, Johnson R. 2000. Cross-hole electrical imaging of a controlled saline tracer injection. *Journal of Applied Geophysics* **44**(2–3): 85–102.

Toto EA, Kerrouri C, Zouhri L, El Basri M, Ibenbrahim A, Mohamad H, Benammi M. 2008. Geoelectrical exploration for groundwater in Al Maha Forest, Ain Jouhra, Morocco. *Hydrological Processes* **22**(11): 1675–1686.

Tsokas G, Tsourlos P, Papadopoulos N, Manidaki V, Ioannidou M, Sarris A. 2006. Non-destructive ERT survey at the south wall of Akropolis of Athens, Greece. In *Near Surface* Helsinki, Finland. Expanded Abstracts, B040.

Tsokas GN, Tsourlos PI, Vargemezis G, Novack M. 2008. Non-destructive electrical resistivity tomography for indoor investigation: the case of Kapnikarea Church in Athens. *Archaeological Prospection* **15**(1): 47–61.

Uhlenbrook S, Didszun J, Wenninger J. 2008. Source areas and mixing of runoff components at the hillslope scale—a multi-technical approach. *Hydrological Sciences Journal* **53**(4): 741–753.

Van PV, Park SK, Hamilton P. 1991. Monitoring leaks from storage ponds using resistivity methods. *Geophysics* **56**: 1267–1270.

Westbrook SJ, Rayner JL, Davis GB, Clement TP, Bjerg PL, Fisher SJ. 2005. Interaction between shallow groundwater, saline surface water and contaminant discharge at a seasonally and tidally forced estuarine boundary. *Journal of Hydrology* **302**(1–4): 255–269.

Wright PM, Ward SH, Ross HP, West RC. 1985. State-of-the-art geophysical exploration for geothermal resources. *Geophysics* **50**: 2666–2699.

Zouhri L, Gorini C, Mania J, Deffontaines B, Zerouali A. 2004. Spatial distribution of resistivity in the hydrogeological systems, and identification of the catchment area in the Rharb basin, Morocco. *Hydrological Sciences Journal* **49**(3): 387–398.

